Available online at www.sciencedirect.com
SCIENCE DIRECT®
ELSEVIER
Optics and Lasers in Engineering 44 (2006) 1209–1218
OPTICS and LASERS in ENGINEERING

# Interpretation of fringes produced by time average reflection moiré on a circular disk

Minvydas Ragulskis[a,*], Loreta Saunoriene[a], Jurate Ragulskiene[b]

[a]*Department of Mathematical Research in Systems, Kaunas University of Technology, Studentu 50-222, Kaunas LT-51368, Lithuania*
[b]*Department of Technical Sciences, Kaunas College, Pramones pr. 20, Kaunas LT-50468, Lithuania*

Received 1 March 2005; received in revised form 1 August 2005; accepted 1 October 2005
Available online 1 December 2005

**Abstract**

Inverse problem of reconstruction of dynamic displacements from the fringe pattern generated by time average reflection moiré is investigated in this paper. A technique for numerical simulation of time average smoothed reflection moiré fringes is proposed. The smoothing procedure is incorporated into the finite element formulation of the problem. Reconstruction of the field of deflections is illustrated for a centrally clamped disk. Such techniques can be effectively exploited in hybrid numerical–experimental procedures for different objects and grating geometries.


*Keywords:* Reflection moiré; Time average; Fringes; Inverse problem

## 1. Introduction

The problem of bending vibrations is common in different engineering and physical applications. Bending vibrations of centrally clamped rotating circular disks play crucial role in the functionality of hard disk drives [1,2]. Lot of efforts are spent for dynamic stabilisation, control and measurement of bending vibrations in such micro-mechanical systems [3].

*Corresponding author. Tel.: +370 698 22456; fax: +370 373 30446.
*E-mail address:* Minvydas.Ragulskis@ktu.lt (M. Ragulskis).

0143-8166/$ - see front matter 
doi:10.1016/j.optlaseng.2005.10.006

Nevertheless, measurement of microscopic deflections from the state of equilibrium is a challenging problem. Different optical measurement techniques are developed for experimental investigation of bending vibrations [4]. Reflection moiré is one of the popular methods for experimental analysis of bending vibrations of structures.

Unfortunately, interpretation of experimental measurement results is a non-trivial inverse engineering problem often having non-unique solutions [5]. This is especially relevant for time average reflection moiré applied for circular structures. Interpretation of fringes generated by time average techniques is already a challenging problem. The problem gets only more complex if the grating lines are circular.

Therefore, there exists a definite need for hybrid numerical–experimental techniques [5,6] that could help to interpret the measurement results. Such techniques usually comprise a numerical model of the system coupled with optical and geometrical parameters of the measurement set-up. Then the predicted response of the experimental optical measurement system can be mimicked in virtual numerical environment when the dynamical parameters of the analysed object are pre-defined. Visualisation techniques of the results from finite element analysis are important due to several reasons. First is the meaningful and accurate representation of processes taking place in the analysed structures. Second, and perhaps even more important, is building the ground for the previously mentioned hybrid numerical–experimental techniques.

## 2. The model of the system

The principle of the reflection moiré analysis [4] is presented in Fig. 1 where $x$, $y$ and $z$ denote the axes of the Cartesian frame ($y$ axis is not shown for simplicity). The clamped circular disk in the status of equilibrium is in the plane $x$–$y$. It is assumed that an ideal mirror film covers the surface of the disk. Moiré grating and the photographic plate are parallel to the plane $x$–$y$. The distance between the photographic plate and the analysed disk is $d$. The deflection of the plate is $w$. It is assumed that the analysed vibrations are small and that $d \gg w$. The subscript denotes partial derivative; $\boldsymbol{N}$ is the normal vector to the surface of the disk; $u$ and $v$ denote $x$- and $y$-shifts of the reflected moiré grating with respect to the reflected moiré grating in the status of equilibrium (shift $v$ is not shown in Fig. 1). This is a schematic representation of an optical set-up for reflection moiré analysis. Real experimental implementation would require a semi-silvered mirror to be introduced in order to assure that the moiré grating and the photographic plate would not overlap each other [4]. Nevertheless, this would not alter the physical processes taking place in the optical set-up and the simplified schematic representation can be used for the numerical simulations.

## 3. Construction of the digital reflection moiré images

Finite element techniques [7] are used to construct the numerical model of a centrally clamped circular disk. Plate bending element with the independent interpolation of the displacement $w$ and the rotations about the appropriate axes

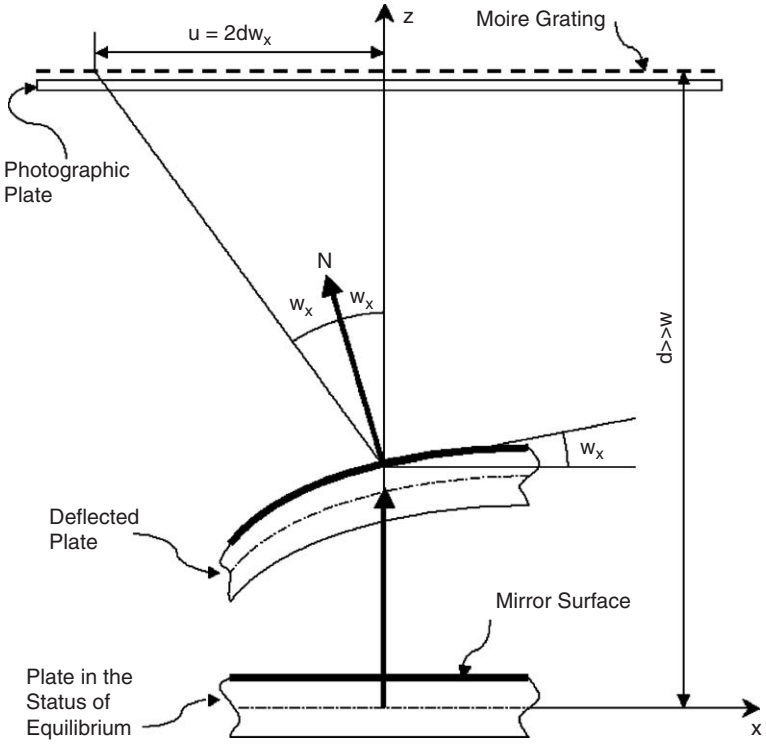


Fig. 1. Schematic diagram of reflection moiré measurement set-up.

$\theta_x$ and $\theta_y$ is used [7]. Formation of digital reflection moiré images requires nodal components of the derivatives of the deflection $w$. Therefore, nodal derivatives of the transverse displacement must be calculated.

The derivatives of the deflection at the points of numerical integration of the finite element are calculated in the usual way:

$$\begin{Bmatrix} w_x \\ w_y \end{Bmatrix} = [B]\{\delta_0\}, \tag{1}$$

where $\{\delta_0\}$ is the vector of nodal displacements, $w_x$ and $w_y$ are the derivatives of $w$ in $x$ and $y$ directions, and $[B]$ is the matrix relating the derivatives with the deflections:

$$[B] = \begin{bmatrix} \dfrac{\partial N_1}{\partial x} & 0 & 0 & \cdots & \dfrac{\partial N_n}{\partial x} & 0 & 0 \\ \dfrac{\partial N_1}{\partial y} & 0 & 0 & \cdots & \dfrac{\partial N_n}{\partial y} & 0 & 0 \end{bmatrix}, \tag{2}$$

where $N_i$ are the shape functions of the finite element and $n$ is the number of nodes of the finite element.

Conventional FEM analysis techniques are based on the approximation of nodal deflections (not their derivatives) via the shape functions [7,8]. Though the field of deflections is continuous in the global domain (also at inter-element boundaries), the calculated derivatives are discontinuous due to the operation of differentiation (Eq. (2)). As the pattern of reflection moiré fringes is sensitive to the derivatives of deflections [4], there exists a need to develop a technique for smoothing the field of those derivatives. Applicability of conventional FEM would be inappropriate due to extremely dense meshing required for production of sufficiently smooth pattern of fringes. Smoothing technique based on conjugate approximation of the field of stresses [6] is adapted for the problem of reflection moiré. Moreover, the smoothing technique must handle data from dynamic analysis (the object of research is time average reflection moiré).

First of all, the eigenmodes of the structure are computed using conventional FEM displacement formulation. It is assumed that the structure performs harmonic vibrations according to one of the eigenmodes (the vibration energy is concentrated in one eigenmode). The appropriate eigenmode of derivatives of deflections is obtained by minimising the following residuals:

$$\begin{aligned}
&\frac{1}{2}\iint\left(([N]\{\delta_x\}-w_x)^2+\mu\left(\left(\frac{\partial w_x}{\partial x}\right)^2+\left(\frac{\partial w_x}{\partial y}\right)^2\right)\right)\mathrm{d}x\,\mathrm{d}y,\\
&\frac{1}{2}\iint\left(([N]\{\delta_y\}-w_y)^2+\mu\left(\left(\frac{\partial w_y}{\partial x}\right)^2+\left(\frac{\partial w_y}{\partial y}\right)^2\right)\right)\mathrm{d}x\,\mathrm{d}y,
\end{aligned}\tag{3}$$

where $\mu$ is the smoothing parameter, $\{\delta_x\}$ the vector of nodal values of $w_x$, $\{\delta_y\}$ the vector of nodal values of $w_y$, and $[N]$ is the row of the shape functions of the finite element:

$$[N]=[N_1,\ N_2\ \ \ldots N_n].\tag{4}$$

Keeping in mind that the terms $\mu((\partial w_x/\partial x)^2+((\partial w_x/\partial y))^2)$ and $\mu((\partial w_y/\partial x)^2+((\partial w_y/\partial y))^2)$ can be approximated as $\mu\{\delta_x\}^{\mathrm{T}}[B^*]^{\mathrm{T}}[B^*]\{\delta_x\}$ and $\mu\{\delta_y\}^{\mathrm{T}}[B^*]^{\mathrm{T}}[B^*]\{\delta_y\}$, respectively [10], step by step differentiation of Eq. (3) leads to the following systems of linear algebraic equations for the determination of each of the components of the derivatives:

$$\begin{aligned}
&\iint([N]^{\mathrm{T}}[N]+[B^*]^{\mathrm{T}}\mu[B^*])\,\mathrm{d}x\,\mathrm{d}y\cdot\{\delta_x\}=\iint[N]^{\mathrm{T}}w_x\,\mathrm{d}x\,\mathrm{d}y,\\
&\iint([N]^{\mathrm{T}}[N]+[B^*]^{\mathrm{T}}\mu[B^*])\,\mathrm{d}x\,\mathrm{d}y\cdot\{\delta_y\}=\iint[N]^{\mathrm{T}}w_y\,\mathrm{d}x\,\mathrm{d}y,
\end{aligned}\tag{5}$$

where $[B^*]$ is the matrix of the derivatives of the shape functions (the first row with respect to $x$; the second with respect to $y$):

$$[B^*] = \begin{bmatrix} \frac{\partial N_1}{\partial x} & \frac{\partial N_2}{\partial x} & \cdots & \frac{\partial N_n}{\partial x} \\ \frac{\partial N_1}{\partial y} & \frac{\partial N_2}{\partial y} & \cdots & \frac{\partial N_n}{\partial y} \end{bmatrix}. \tag{6}$$

The technique of the selection of the magnitude of the smoothing parameter is based on average finite element error norms [6]. When the smoothing parameter is too small, the images are insufficiently smooth because of the strains calculated from the displacement formulation. When the parameter is too big, an over-smoothed image is obtained which can be far from the experimental reflection moiré image.

Digital formation of the time average reflection moiré images is similar to the problems of time average geometric moiré, which are described in detail in [9]. The formation of fringes in reflection moiré is sensitive to deflection derivatives [4]. Thus, the difference between the reflection moiré and geometric moiré [4] is that instead of dynamic displacements $u$ and $v$, the following values are used in the reflection moiré:

$$u = 2dw_x, \quad v = 2dw_y. \tag{7}$$

## 4. Analysis of centrally clamped disk

Finite element mesh and the tenth eigenmode of a centrally clamped disk are shown in Fig. 2. The mesh in the status of equilibrium is grey and deflected according to the eigenmode is black. Isolines of the partial derivatives of the dynamic

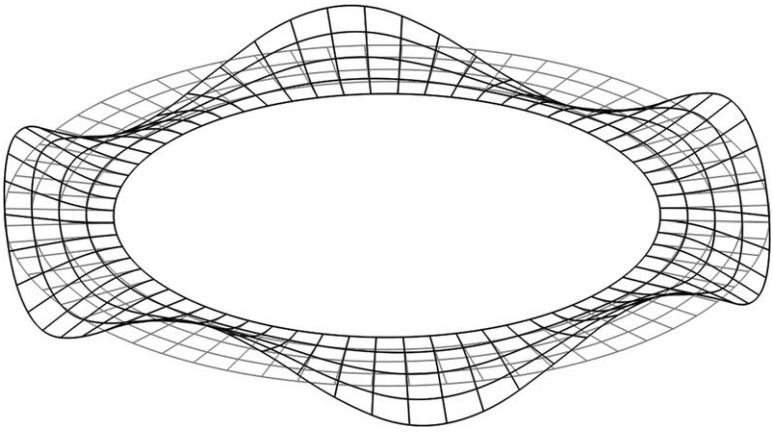

Fig. 2. The tenth eigenmode of the centrally clamped disk.

displacement in radial and angular directions are presented in Fig. 3a and b. Smoothed isolines ($\mu = 0, 1$) of the partial derivatives of the dynamic displacement are presented in Fig. 4a and b. It can be noted that rather small smoothing enables to avoid unphysical breakings of the isolines.

Time average reflection moiré images are presented in Fig. 5a and b for radial and angular gratings, respectively. It can be noted that the correspondence between the pattern of fringes and the isolines is evident.

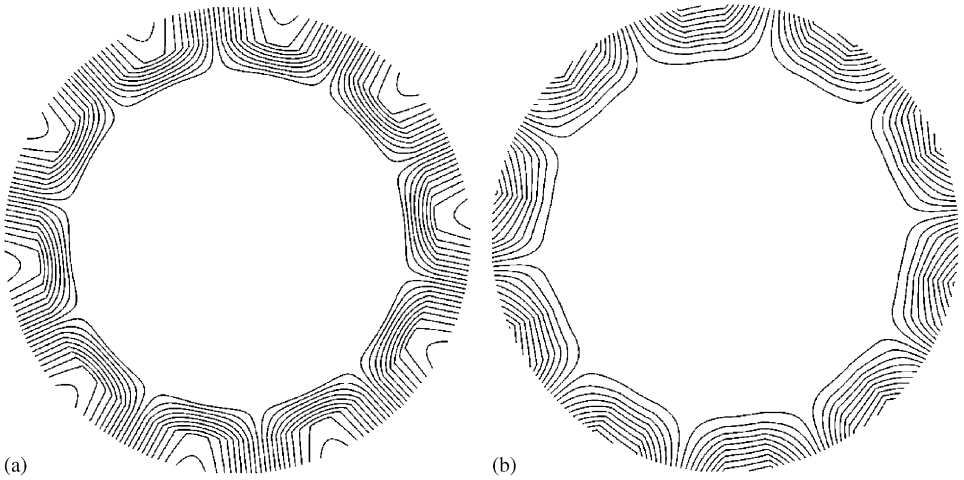


Fig. 3. Unsmoothed isolines of the derivatives of the deflection (a–in the radial direction; b–in the angular direction).

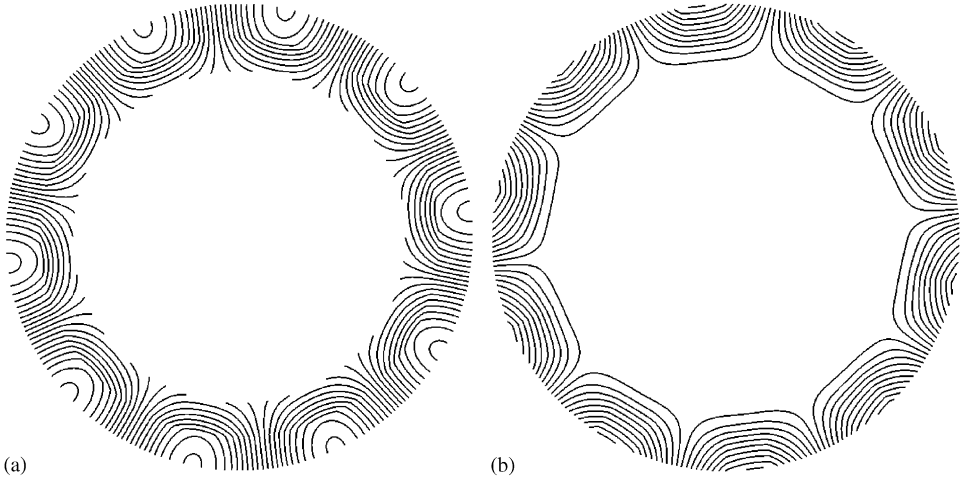


Fig. 4. Smoothed isolines of the derivatives of the deflection (a–in the radial direction; b–in the angular direction).

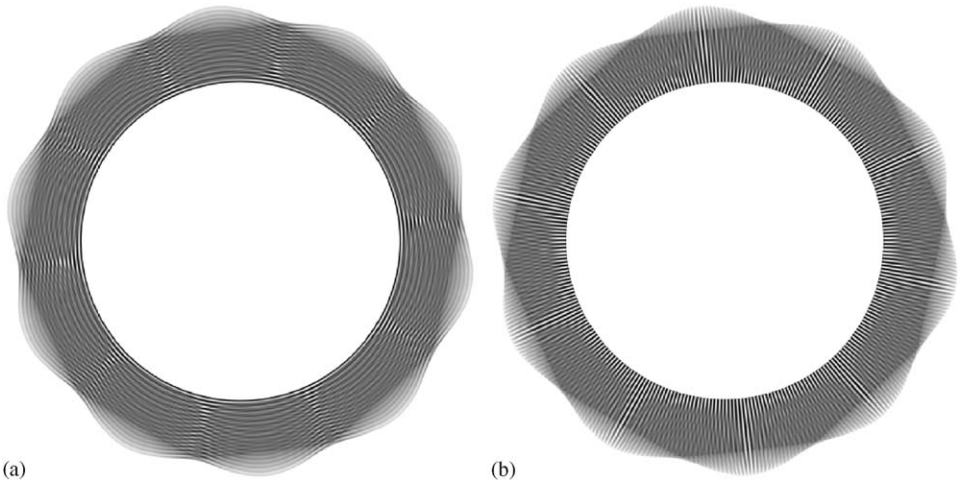


Fig. 5. Time average reflection moiré images (a–radial grating; b–angular grating).

## 5. Quantitative analysis of dynamic deformations

Time average fringe-based experimental methods can be effectively applied for the analysis of dynamic deformations. A typical example when time average geometric moiré is applied for measurement of plane motions is presented in [9]. The explicit relationship among the fringe order $n$, pitch of the grating $\lambda$ and dynamic one-dimensional displacement $u$ is [9]

$$u = \frac{\lambda}{2\pi} b_n, \tag{8}$$

where $b_n$ is the $n$th root of the zero-order Bessel function of the first kind. The values of the roots of the zero order Bessel function of the first kind are available in classical texts [10].

Time average reflection moiré analysis is sensitive to bending vibrations, not plane motions. But analogous relationship can be constructed taking into account Eq. (7):

$$w_x = \frac{\lambda}{4\pi d} b_n. \tag{9}$$

It can be noted that the component $w_y$ can be reconstructed in a similarway but using a mutually orthogonal grating. In general, all optical moiré techniques can be used to reconstruct physical quantities in the direction orthogonal to the lines of the gratings [4]. If the grating lines are circular in the analysed problem of centrally clamped disk, only the radial derivative of deflection $w_r$ can be reconstructed using such a grating.

The goal of experimental analysis of bending vibrations of a clamped disk is to determine the field of dynamic deflections, not their derivatives. Keeping in mind

that the internal radius of the disk $r_0$ is fastened, the dynamical deflections can be reconstructed integrating the approximated derivatives:

$$w(r) = \int_{r_0}^{r} W_r(r)\,\mathrm{d}r, \tag{10}$$

where $W_r(r)$ is an approximated polynomial over the discrete values of $w_r$ at the centres of interference fringes.

The procedure of the reconstruction of dynamic deflections from the pattern of interference fringes is illustrated by the following example. First of all, the derivatives of the deflections at the centres of interference fringes must be determined. This requires application of the fringe counting technique [4]; then Eq. (9) can be used to calculate the discrete values of the derivatives of the deflection.

The zoomed part of the pattern of fringes produced by time average mirror moiré for the tenth eigenmode of the internally clamped disk is presented in Fig. 6. Dynamic deflections are reconstructed along an axial line going through the area of maximum deflections. Fringe counting is straightforward due to the fact that the internal radius of the disk is fastened; fringe orders are shown at the appropriate intersections of fringes and the axial line. The clamped internal radius of the disk is 100 mm, free external radius is 140 mm and the width of the analysed disk section is 40 mm. Pitch of the grating $\lambda = 2.5$ mm; distance between the photographic plate and the clamped disk $d = 100$ mm. For simplicity, it is assumed that the parameter $r$

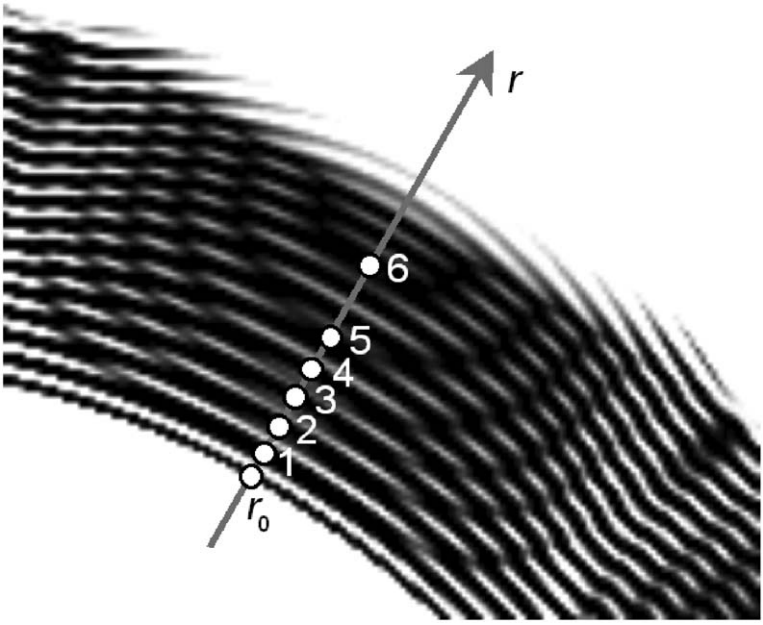


Fig. 6. Zoomed time average reflection moiré image with radial grating.

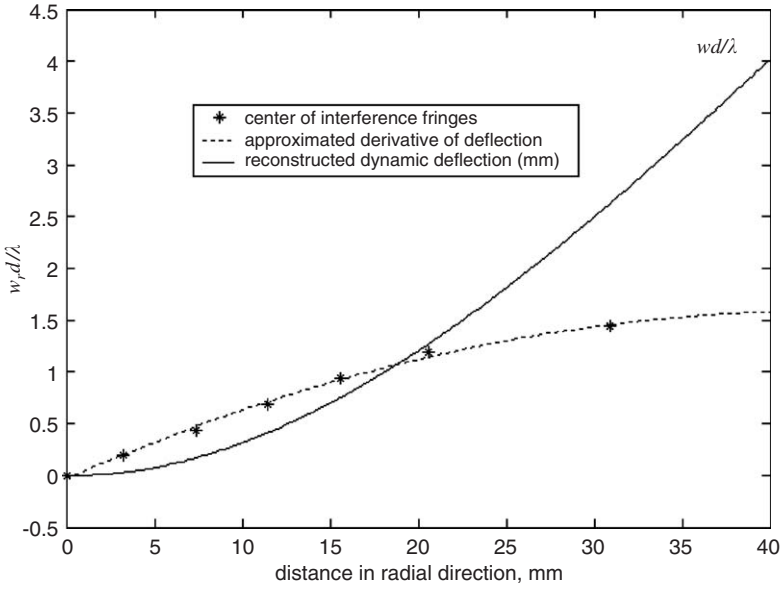


Fig. 7. Reconstruction of the dynamic deflection.

is equal to 0 at the point where the internal radius of the disk is fastened ($r_0 = 0$). Then the analysed range of $r$ is between 0 and 40 mm.

The discrete values of the derivative of the deflection are calculated at appropriate intersection points (Fig. 7), where $x$-coordinates of the points are calculated from Fig. 6 and $y$-coordinates from Eq. (9). Next step is the approximation of continuous deflection derivative function $W_r(r)$ through the discrete values of $w_r$ (Fig. 7). Some scattering of points around the approximated polynomial can be explained by the measurement errors of the centres of interference fringes. Finally, dynamic deflections of the clamped disk can be reconstructed integrating the approximated polynomial (Eq. (10)). The produced curve (Fig. 7) characterises the dynamic behaviour of the disk. Good adequacy between the reconstructed dynamic deflections and the geometrical shape of the disk in its extreme deflection (Fig. 2) validates the presented procedure.

## 6. Concluding remarks

A whole set of problems had to be solved before the numerical construction of moiré fringes was possible. First of all, the image smoothing procedures had to be developed for the reflection moiré analysis due to the fact that the displacement-based (not deflection derivative based) finite element methods were used for the description of investigated engineering structures. Secondly, digital time averaging techniques had to be applied in order to generate fringe patterns corresponding to

time average reflection moiré fringes. Finally, techniques for solving the inverse problem of the reconstruction of the deflections from the pattern of fringes had to be developed.

The presented technique for interpretation of fringes is applicable in hybrid numerical–experimental time average reflection moiré analysis of bending vibrations of different engineering structures and shows the complexity of the inverse problem of the reconstruction of dynamic displacements. Such techniques can help to analyse and interpret optical experimental results with greater precision.

## References

[1] Naganathan G, Ramadhayani S, Bajaj AK. Numerical simulations of flutter instability of a flexible disk rotating close to a rigid wall. J Vib Control 2003;9(1–2):95–118.
[2] Tian J, Hutton SG. Travelling-wave modal identification based on forced or self-excited resonance for rotating discs. J Vib Control 2001;7(1):3–18.
[3] Manzione P, Nayfeh AH. Instability mechanisms of a centrally clamped rotating circular disk under a space-fixed spring-mass-dashpot system. J Vib Control 2001;7(7):1013–34.
[4] Kobayashi AS, editor. Handbook on experimental mechanics. 2nd ed. SEM; 1993.
[5] Holstein A, Salbut L, Kujawinska M, Juptner W. Hybrid experimental–numerical concept of residual stress analysis in laser weldments. Exp Mech 2001;41(4):343–50.
[6] Ragulskis M, Ragulskis L. Plotting isoclinics for hybrid photoelasticity and finite element analysis. Exp Mech 2004;44(3):235–40.
[7] Bathe KJ. Finite element procedures in engineering analysis. New Jersey: Prentice-Hall; 1982.
[8] Huebner KH, Dewhirst DL, Smith DE, Byrom TG. Finite element method. New York: Wiley; 2001.
[9] Ragulskis M, Maskeliunas R, Ragulskis L, Turla V. Investigation of dynamic displacements of lithographic press rubber roller by time average geometric moiré. Opt Lasers Eng 2005;43(9):951–62.
[10] West CM. Holographic interferometry. New York: Wiley; 1979.